Journal of Applied Fluid Mechanics, Vol. 16, No. 1, pp. 179-191, 2023.
Available online at www.jafmonline.net, ISSN 1735-3572, EISSN 1735-3645.
https://doi.org/10.47176/jafm.16.01.1345

Visual Comparative Analysis for the Oil-air Two-Phase Flow of An Oil-Jet Lubricated Roller-Sliding Bearing

J. J. Zhang, L. M. Lu†, Z. Y. Zheng, L. Gan and Z. Y. Lv

Key Laboratory of Conveyance and Equipment Ministry of Education, East China Jiaotong University, Nanchang 330013, China

†*Corresponding Author Email: 1199@ecjtu.edu.cn*

(Received June 6, 2022; accepted September 18, 2022)

ABSTRACT

To discuss the lubrication characteristics of roller-sliding bearing under oil-injected lubrication, the CFD method was introduced into the fluid-structure interaction model to realize the transient simulation of oil-air two-phase flow (OATPF). The volume of fluid (VOF) method is applied to capture the oil-air interface. A sliding mesh is established between the inner flow field and outer flow field. Moreover, the two design schemes of roller-sliding bearing are compared. A reasonable design scheme is obtained. The bearing rotation speed, oil velocity, oil viscosity, oil ratio, and oil temperature have a significant impact on the lubrication performance of the roller-sliding bearing. The results show that the oil distribution inside the bearing is uneven. The lowest oil volume fraction exists in the basin, which is near the upstream of the nozzle, and gradually increases from the inner raceway to outer raceway. The oil storing rate increases with the increase of oil viscosity. A novel method of oil volume prediction is proposed in a deep manner. It also provides some reference for the design of roller-sliding bearing and other bearings.

Keywords: Roller-sliding bearing; Oil injection; Oil-air two-phase flow; Fluid distribution; CFD.

1. INTRODUCTION

The roller-sliding bearing is a new type of bearing evolved from cylindrical roller bearing and floating-ring sliding bearing. Its structure mainly consists of an outer ring, roller, slider, and inner ring. It is especially suitable for intermittent motion and frequent start and other working occasions (Lu 2013, 2019). For roller-sliding bearing, traditional lubrication methods are not suitable for it, such as pure oil or grease. Under pure oil lubrication, the bearing will generate a lot of heat due to movement of sliding and roller. With the situation of grease lubrication, lubrication will be lost due to scrap and squeeze on the slider, which increases friction torque (Lu *et al.* 2021). The roller-sliding bearing often operates under cyclic loads. It will be a challenge to improve its lubrication characteristics. Therefore, it is important to research the oil-injection lubrication performance of roller-sliding bearing.

Owing to the great complex nature of flow field during the lubrication process, the complete calculation theory has not been given yet. In early stage, the elastohydrodynamic (EHD) lubrication theory was mainly used to describe the formation mechanism of bearing oil film, and a relatively complete theoretical system was formed (Chao-Ho and Rong-Tsong 1994; Chu *et al* 2010; Chu *et al* 2012; Zhang 2006; Meng and Chen 2015; Feidt 2012; Awasthi *et al* 2014; Wei *et al* 2015; Chu *et al.* 2010). However, the elastohydrodynamic (EHD) lubrication theory is a calculation derived from many preconditions and has good accuracy in characterizing lubrication contact, but it has great limitations in describing fluid motion in whole areas of the bearing. With the progress of computational techniques and fluid mechanics, CFD techniques have been widely used in various scenarios of fluid analysis. Gao *et al.* (2019) investigated the distribution of two-phase flow in cylindrical roller bearings using CFD. Under oil injection lubrication conditions, the flow of fluid inside the bearing is traced using the VOF model to determine the optimal lubrication conditions. It was found that bearing speed, lubricant density and fluid volume have a large effect on the oil distribution inside the bearing. Concli *et al.* (2020) proposed a new method to simulate the internal oil-air distribution of cylindrical roller bearings using OpenFOAM CFD software. The computational efficiency of the model was mainly discussed, rather than analyzing the performance of the bearings themselves. Aiming at the problem of complex structured mesh strategy, different models were simplified and analyzed. The results show that for a highly symmetric bearing

model, the calculation efficiency can be improved by ignoring the rounding radius and establishing the three-dimensional model of part of bearing region. In 2019, Marchesse *et al.* (2019) conducted a similar study on cylindrical roller bearings. The authors consider the variation of fluid viscosity and fluid density inside the bearing, where different densities and viscosities correspond to different oil and air phases to realize the simulation of two-phase flow. By analyzing the results of the bearing dynamic simulation, they found that the change of oil-phase volume has greatly influenced the stability of fluid motion. Wang *et al.* (2017) applied ANSYS Fluent to conduct a numerical simulation of fluid movement and discussed the fluid distribution in the sliding bearing. The simulation analyzed the dynamic characteristic coefficients through the dynamic mesh technique. The visualization results show that the variation of the bearing speed is with a vital role in the oil film stiffness. The damping factor has little effect on the changes in rotational speed. Lu *et al.* (2020) proposed a CFD simulation technique for analyzing the two-phase flow of roller-sliding bearing. The simulation details are limited, but the effect of pipe angle on the oil-air two-phase distribution in the flow field is considered. The results show that the two-phase flow of oil and air has a good lubricating work and is suitable for roller-sliding bearings. As the angle of the pipe increases, the agitation in the bearing becomes more severe, which affects the stability of the lubricating film.

The keywords in the references were exported in the Scopus database. A correlation analysis was carried out on the research topics in the literature (See in Fig. 1). The wider the dot area, the stronger the correlation. Therefore, the above research shows that it is feasible to apply CFD technology to study the roller-sliding bearing.

This paper focuses on the prediction of oil phase volume and oil storing rate under jet-lubrication based on the roller-sliding bearing model. In addition, this study compares the oil-air distribution, oil storing rate in the bearing cavity, slider pressure, and air pressure of two schemes, taking into account bearing rotation speed, oil velocity, oil volume fraction, oil ratio, oil temperature and oil viscosity. A novel method of oil-phase volume prediction is proposed in a deep manner. According to the literature review, this model is with little researches about this configuration. Therefore, there is a need to study its ability to assess dissipation in a correct manner. Due to the consideration of high-speed conditions, it can be demonstrated that the roller-sliding bearing model with a relatively higher oil-phase volume. The purpose of this study is to obtain a more accurate oil-phase volume in this model by using the CFD method, which will be introduced later.

The organization of the article are listed below. First, the lubrication mechanism of the roller-sliding bearing is described. Then the equation of the VOF model is elaborated and the prediction method of the roller-sliding bearing is proposed. A slip mesh model was introduced for numerical evaluation of oil volume transfer. Finally, the oil volume fraction is discussed.

2. DESCRIPTION OF THE LUBRICATION MECHANISM

As shown in Fig. 2(a), it is a two-dimensional schematic of the lubricated process of the roller-sliding bearing. During oil injection lubrication, lubricant is sprayed into the inner cavity through a tiny nozzle. In the lubrication process, the lubricant flows roughly in three ways: due to the centrifugal force generated by the bearing rotation, part of lubricant can be removed from the bearing; in addition to the mutual movement between the slider and the roller, the bearing cavity may also remain some lubricant; due to initialization, some remaining lubricant may move axially along the inner raceway. The associated lubricant streamline is shown in Fig. 2(b).

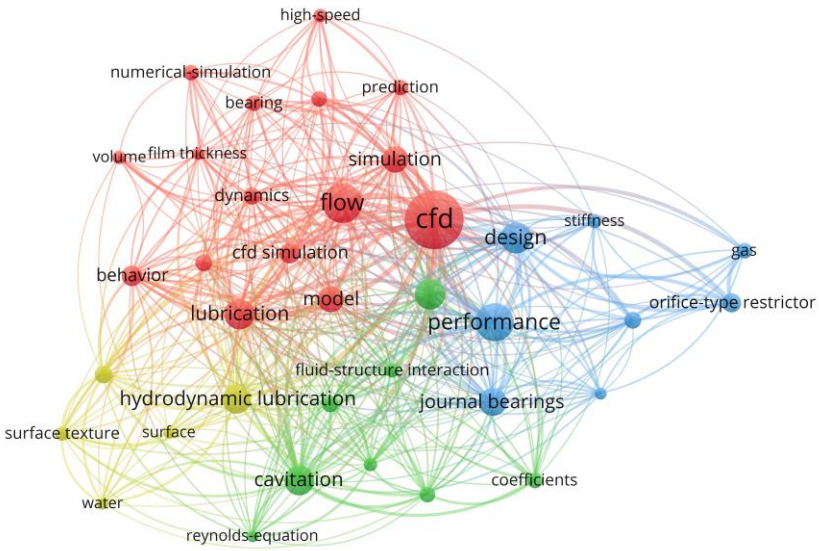

Fig. 1. Network visualization of keywords in the references.

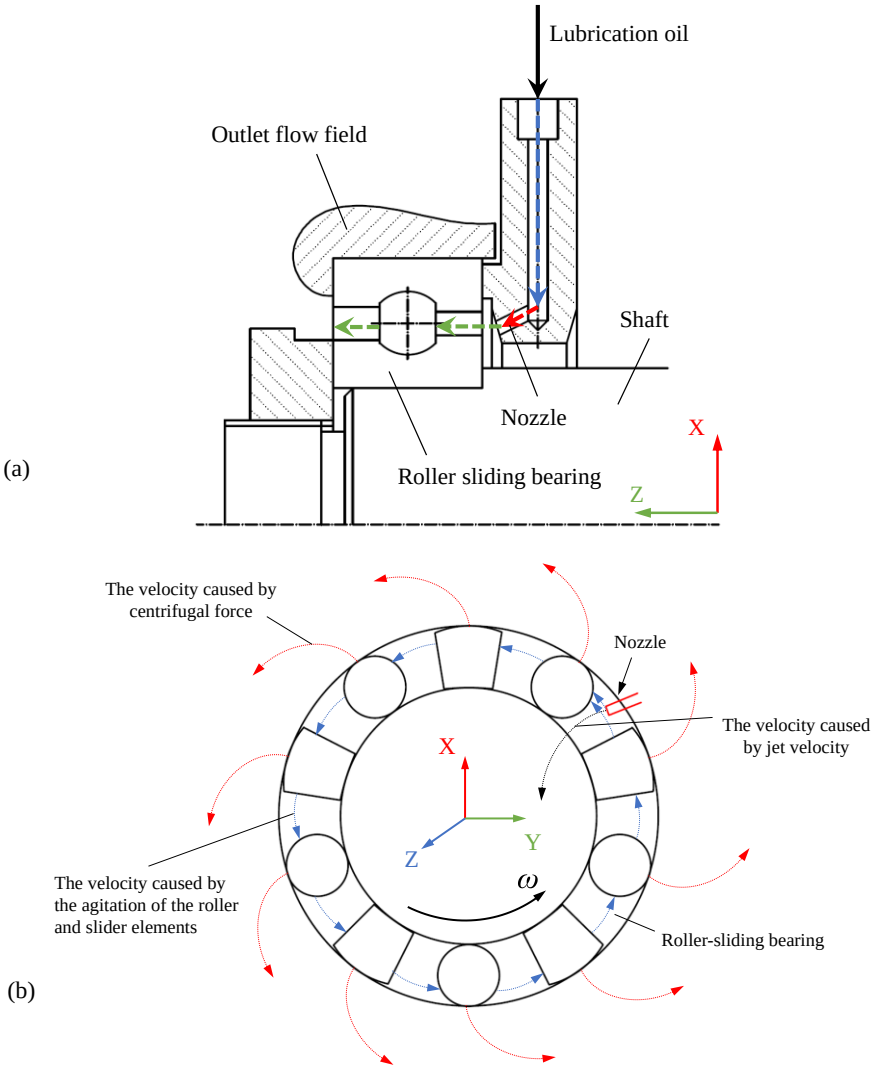

Fig. 2. Lubrication system. (a) Schematic diagram of lubrication mode of roller-sliding bearing; (b) Relative streamline of lubricating oil.

3. MATHEMATICAL MODEL AND NUMERICAL METHOD

3.1 Two-phase Flow Mode

In the lubrication process, oil-air two-phase flow is involved in the roller-sliding bearing. Therefore, the VOF method is applied to obtain the oil-air distribution. In 1981, Hirt and Nichols proposed the VOF method (Hirt and Nichols 1981). As a fluid analysis method, the VOF technique is relatively accurate, small error, and capable of solving highly complex flow fields (Mehdizadeh *et al.* 2011).

In the VOF method, the oil-phase volume fraction(φ_{oil}) is expressed as follows: $\varphi_{oil}=0$ and $\varphi_{oil}=1$ indicate that there are no oil phase and full of the oil phase in the control body respectively; $0<\varphi_{oil}<1$ denotes that the control body is with a state of oil-air mixture. Therefore, the φ_{oil} is defined as:

$$\begin{cases} \varphi_{oil}=0 & \text{air phase} \\ \varphi_{oil}=1 & \text{oil phase} \\ 0<\varphi_{oil}<1 & \text{interface} \end{cases} \tag{1}$$

To trace the oil-air interface, the continuity equation needs to be solved. The continuity equation is described by:

$$\frac{\partial}{\partial t}(\varphi_{oil}\rho_{oil})+\nabla\cdot(\varphi_{oil}\rho_{oil}\vec{v})=S_{\alpha_{oil}} \tag{2}$$

Where $\vec{v}$, ρ_{oil} and $S_{\alpha_{oil}}$ are the velocity vector, oil density, and mass source terms, respectively (Ramdin and Henkes 2012; Banerjee *et al.* 2002).

In the solving process, Eq. (2) can only be solved for oil-phase volume fraction, conversely, the air-phase volume fraction is obtained from the constraint, which is given by:

$$\varphi_{oil}+\varphi_{air}=1 \tag{3}$$

Where φ_{oil} and φ_{air} are the oil-phase volume fraction and air-phase volume fraction, respectively. In the VOF method, the same momentum equation based on the oil-air two-phase flow (OATPF) property is described as:

$$\frac{\partial}{\partial t}(\rho\vec{v})+\nabla\cdot(\rho\vec{v}\vec{v})= -\nabla p+\rho\vec{g}+\nabla\cdot[\mu(\nabla\vec{v}+\nabla\vec{v}^{T})]+\vec{F} \tag{4}$$

Where ρ, $\vec{g}$, p, $\vec{F}$,and μ are the density of oil-air phase, gravitational acceleration vector, pressure, volumetric force vector, and dynamic viscosity (Da Riva *et al.* 2012).

The two-phase flow solves the same energy equation to obtain the fluid properties, which can be expressed as follows:

$$\frac{\partial}{\partial t}(\rho E)+\nabla\cdot[(p+\rho E)\vec{v}]= \nabla\cdot\left(k_{eff}\nabla T-\sum_{q}\sum_{j}h_{j,q}J_{j,q}+(\vec{\tau}_{eff}\cdot\vec{v})\right)+S_{h} \tag{5}$$

Where k_{eff} is the effective thermal conductivity, $h_{j,q}$ is the enthalpy of substance j in phase q, and $J_{j,q}$ is the diffusive flux of substance j in phase q, S_h is the volume heat source, and E is the mass-averaged variable.

The mass characteristics of the momentum equation can be identified from the average volume fraction. The fluid properties (dynamic viscosity and density) for mixed phase can be written as:

$$\rho=\varphi_{air}\rho_{air}+\varphi_{oil}\rho_{oil} \tag{6}$$

$$\mu=\varphi_{air}\mu_{air}+\varphi_{oil}\mu_{oil} \tag{7}$$

Where ρ_{air} is the density of air. The μ_{oil} and μ_{air} are with represent of oil-phase dynamic viscosity and air-phase dynamic viscosity, respectively.

During the lubrication process, most of the lubricant flows on the inner raceway, slider and roller. As a result, the interface of the solid and the fluid bends, causing the curvature to change with the flow of the fluid. Therefore, this model considers the wall adhesion angle. The curvature of the local interface can be determined by the static contact angle, which is with the location between the wall and the interface. The wall normal is given by:

$$\vec{n}_a=\vec{n}_w\cos\theta_w+\vec{\tau}_w\sin\theta_w \tag{8}$$

Where $\vec{n}_a$, $\vec{\tau}_w$, and $\vec{n}_w$ are the wall normal vector, the unit tangent vector, and the unit normal vector, respectively.

At different speeds of the bearing, due to the different Reynolds numbers of oil and air, high-speed rotation and eddy currents need to be considered. Therefore, this study considers a relatively higher bearing rotation speed, adopts the k-ε renormalization group (RNG) turbulence model, and considers the high curvature and high stress changes. This model can improve the computational accuracy under turbulent conditions to a certain extent (Xiao *et al.* 2012).

3.2 Slip Mesh Model

For the purpose of analyzing the internal flow field, it is necessary to determine the value of the bearing rotational speed and set the rotational state to transient. Considering the existence of relative motion in the internal and external flow fields, a slip mesh model is applied to the analysis. In this mesh model, the sliding phenomenon occurs at the watershed interface. There is no deformed mesh and mesh reconstruction, which improves the efficiency of the calculation.

The model needs to satisfy momentum conservation and mass conservation. In each step of the calculation, the interface of slip mesh needs to be redefined. The relationship of the flow velocity at any point r with respect to the rotating coordinate system and the fixed coordinate system is described as:

$$\vec{v}_r=\vec{v}-\vec{u}_r \tag{9}$$

$$\vec{u}_r=\vec{\omega}\times\vec{r} \tag{10}$$

Where v_r, v and u_r are the relative velocity, absolute velocity, and implicate velocity, respectively. The governing equations for fluids in rotating coordinates are given by (Hu *et al.* 2014):

$$\frac{\partial\rho}{\partial t}+\nabla\cdot\rho\vec{v}_r=0 \tag{11}$$

$$\frac{\partial}{\partial t}(\rho\vec{v}_r)+\nabla\cdot(\rho\vec{v}_r\vec{v}_r)+\rho(2\vec{\omega}\times\vec{v}_r+\vec{\omega}\times\vec{\omega}\times\vec{r})= -\nabla p+\nabla\cdot\left[\mu(\nabla\vec{v}+\nabla\vec{v}^{T})+\vec{F}\right] \tag{12}$$

Where $2\vec{\omega}\times\vec{v}_r$ and $\vec{\omega}\times\vec{\omega}\times\vec{r}$ are the Coriolis acceleration term and the centripetal acceleration term resulting from the change of bearing rotation speed, respectively.

3.3 Fluid-Structure Coupling Model

In this study, the factors affecting the lubrication characteristics of the roller-sliding bearing are analyzed based on the slider shape. Table 1 shows the specific parameters of the roller-sliding bearing. Fig. 3 shows the design schemes of the roller-sliding bearing. In terms of the slider shape, scheme A is the middle prominent slider, and scheme B is the middle concave slider. But they have the same volume. Please note, this study only considers the case where the outer ring is fixed, the inner ring rotates and the rolling elements do not rotate. The slider is in a linear contact with the inner and outer raceway. In calculation process, the fluid-structure coupling method is applied. The flow chart of fluid-structure coupling simulation is shown in Fig.4. In the coupling process, the inner flow field region and outer flow field region are analyzed separately. The internal flow field analyzes its flow characteristics, and the external flow field analyzes its dynamic characteristics. Then, the coupled analysis of the internal and external flow fields is carried out.

Table 1 Geometric parameters of the roller-sliding bearing.

Parameter	Value
Width (mm)	20
Outer diameter (mm)	90
Ball diameter (mm)	12.186
Inner diameter (mm)	50
Contact angle(degree)	40
Number of balls	7
Number of sliders	7

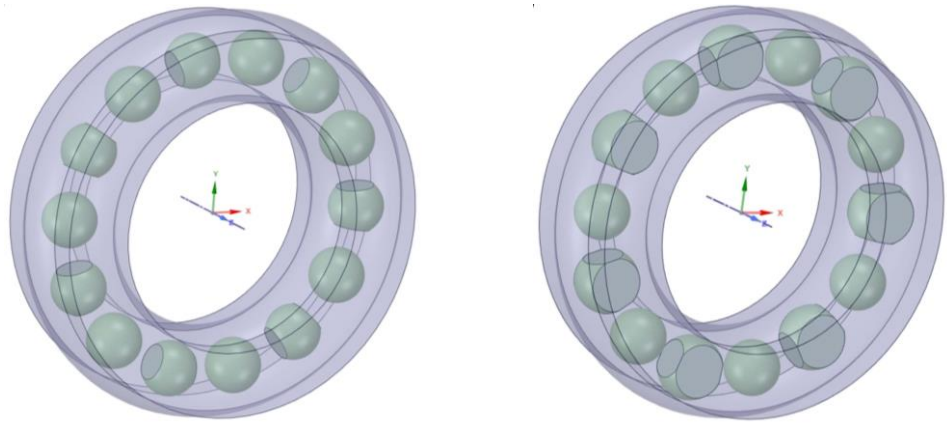

(a) (b)

Fig. 3. Design scheme comparison. (a) Scheme A; (b) Scheme B.

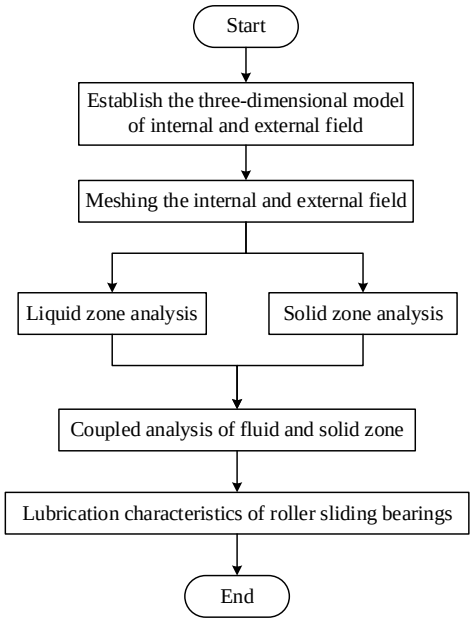

Fig. 4. Flow chart of fluid-structure coupling simulation.

During the calculation, the external flow field is a solid region. The interaction of the fluid and the solid causes the solid to move or deform. In addition, the deformation of the solid can affect the fluid movement, which in turn affects the distribution of the fluid. Figure 5 illustrates the flow mesh model of the roller-sliding bearing, which is a VOF model. According to the description of lubrication mechanism, in this model, two pressure outlets are applied to monitor the flow of lubricant. The nozzles are set up as velocity inflow ports for a single inlet, where velocity is determined by different operating conditions. The bearing surface is set as a pressure outlet and its pressure is set at one standard atmosphere. According to the relative streamline of lubricating oil in Fig. 2(b), the oil flow of two schemes is equal in value. In Fig. 3, in terms of meshing technology, the outer flow field area adopts a hexahedral structured mesh, and the inner flow field area adopts a tetrahedral unstructured mesh, which is proposed with reference to Wu *et al* (2016). Scheme A uses 895,473 cells and Scheme B uses 823,585 cells. The minimum clearance between slider and raceway (inner and outer) is set to 0.25 mm. Meanwhile, a slip mesh is set at the interface of inner and outer fields for data transmission. In order to further reduce the computational errors in the turbulent flow field at the wall, various rotating boundaries are set on different walls. The high Reynolds number region near the wall adopts the standard wall function. However, the low Reynolds number region on the far wall applies the no-slip boundary condition.

Another study was conducted to check the reliability of the model and the accuracy assessment of the numerical solution, a mesh independence test is carried out according to the change of numerical solution. Scheme A and scheme B both use three mesh models with different sizes. Refinement is performed for one index, which means the mesh refinement is based on 2.5 times the initial cell. Table 2 presents the numerical results of mesh independence tests for two schemes. It can be seen

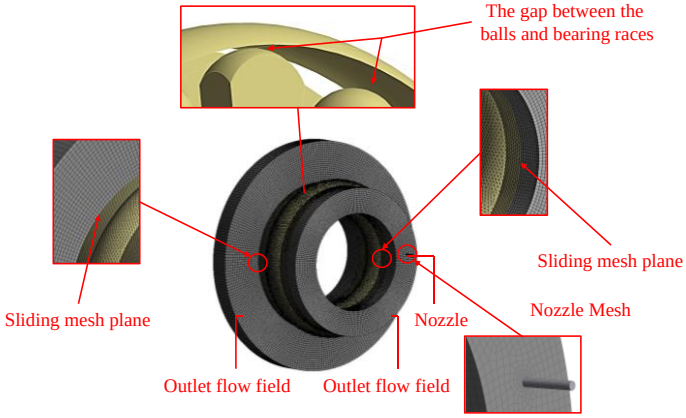

Fig. 5. Flow field mesh of roller-sliding bearing.

Table 2 Mesh independence test for mean oil volume(m^3).

Item	Mesh	Cells number	8000rpm	10000rpm
Scheme A	Mesh1	821.268	0.05415	0.05526
	Mesh2	895.473	0.05421	0.05535
	Mesh3	978.948	0.05434	0.05542
Scheme B	Mesh1	759.372	0.06221	0.06505
	Mesh2	823.585	0.06243	0.06512
	Mesh3	916.256	0.06252	0.06526

that the average oil volume inside the roller-sliding bearing does not change much for different mesh sizes. The average oil difference is less than 5%. The number of meshes has little effect on the numerical results.

3.4 Numerical Methods

When lubricant is sprayed into the bearing, the oil moves along the bearing inner ring. Therefore, it is essential to determine the value of the bearing speed, which is defined by (Harris and Kotzalas 2006):

$$n_b = \frac{1}{2} n \left(1 - \frac{D_b \cos\alpha}{d}\right) \tag{13}$$

Where D_b、n、d、α are the bearing pitch diameter, inner raceway speed, ball diameter, and bearing contact angle, respectively.

In the VOF model, the air phase is set as the incompressible phase as main phase with a density of 1.225kg/m^3 and a viscosity of 1.79×10^5Pa·s respectively. Meanwhile, the oil phase of second phase is a compressible phase with a density of 960 kg/m^3 and the viscosity is constantly changes with the environmental temperature. During initialization, the oil phase functions in the nozzle and bearing cavity are 1 and 0, respectively. The solution process of governing equations is discretized by finite volume method. Phase function equations, second-order windward momentum equations, and turbulence equations are used to accurately describe the motion of fluid. The pressure stage is in PRESTO format. The PISO format is used separately to account for the effect of bearing rotation on fluid flow. Convergence condition is the conservation of import and export masses. In addition, the influencing factors will be discussed as input parameters of the model in the following sections. For example, the bearing speed is the speed of the inner ring of the bearing. The oil viscosity, oil temperature, oil velocity and oil ratio are the oil properties of the oil inlet respectively.

4. Result Analysis

4.1 Analysis of oil-air distribution in roller-sliding bearing

The oil-air distribution in bearing cavity was obtained by numerical simulation, as illustrated in Fig. 6. The bearing rotation speed is 10000r/min, the oil viscosity is 0.14Pa·s, the oil velocity is 18m/s, the oil ratio is 0.9, and the oil temperature is 20℃. According to the distribution of oil-air, the bearing has a stable flow field in the bearing cavity, but the distribution of oil-air is uneven. The oil-phase volume fraction at nozzle is the highest. With the centrifugal force generated by bearing rotation, the high-density oil phase fluid in bearing cavity is concentrated in outer raceway. Therefore, the oil-phase volume fraction in outer raceway is higher than that in inner raceway. The oil-phase volume fraction gradually decreases along the direction of bearing rotation, and the oil-air interface can be observed.

The blue area indicates the air phase, and other colors describe the oil-air phase. In Fig. 6 (a) and Fig. 6 (b), lubricant distribution of scheme B is more uniform than that of scheme A under the same conditions. Most of the lubricant moves in a circular motion around the bearing due to the interaction between the

slider and the roller. The lubricant injected into the bearing surface leaves the cavity from the bearing end face. Therefore, the oil-phase volume fraction is lowest near the upstream of the nozzle. However, the oil-phase volume fraction near the nozzle is higher due to the splash phenomenon between the fluid upstream of the nozzle. Fig.6 (c) shows the average oil-phase volume fraction inside the bearing, which is higher for scheme B compared to scheme A. In summary, in the lubrication process of the roller-sliding bearing, the radial velocity, axial velocity, and circumferential velocity of lubricating oil are not zero. The reason for this is that the centrifugal force affects the radial movement of fluid, the speed of oil injection affects the axial motion of fluid, and the interaction between the slider and the roller will have a greater impact on the circumferential movement of fluid.

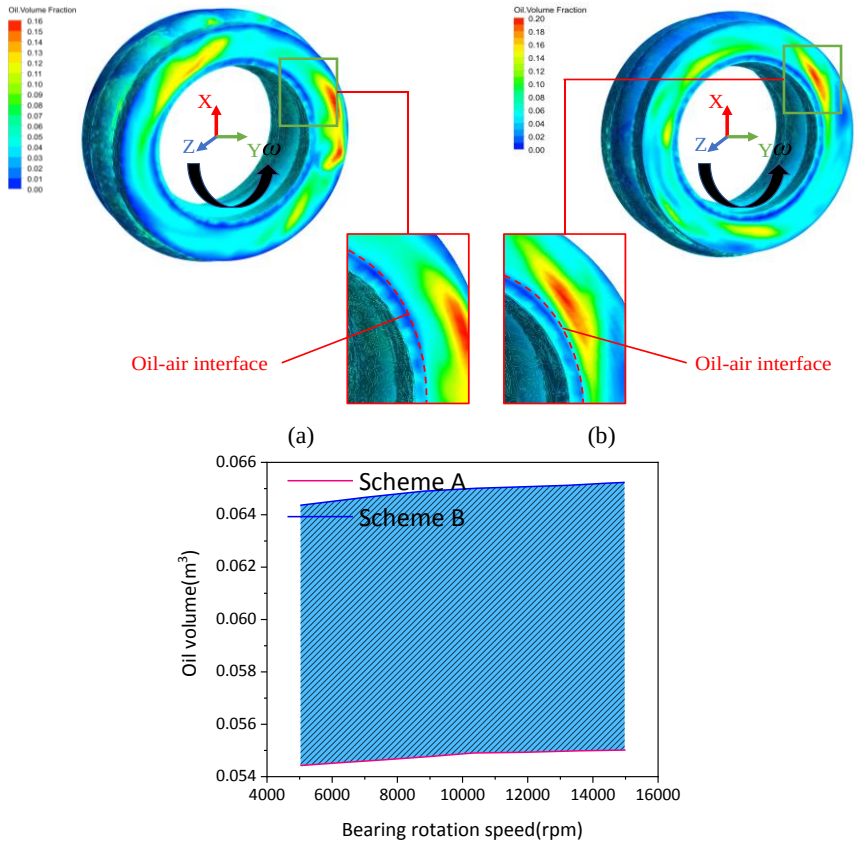

Fig. 6. Average oil-phase volume distribution inside the roller-sliding bearing. (a) Oil-phase distribution of scheme A; (b) Oil-phase distribution of scheme B; (c)Average oil volume in the roller-sliding bearing.

4.2 Influence of Bearing Rotation Speed and Oil Velocity on Bearing Lubrication Characteristics

Figure 7 shows the lubrication characteristics of roller-sliding bearing at different oil velocities and bearing rotation speeds. In this section, the oil temperature is 20 ℃. The lubricant viscosity is 0.14Pa·s. The oil ratio is 0.9. The bearing rotation speed cases are 4000, 6000, 8000, and 10000r/min, respectively. Meanwhile, the oil velocity cases are 18, 28, 38, and 48m/s, respectively. In addition, the oil storing rate in bearing chamber, the bearing rotation speed, the oil velocity, the oil volume and the pressure on slider are considered. Figure 7 (a) and Fig.7 (b) show the effect of bearing rotation speed on oil-phase volume. With the bearing speed increasing, the oil-phase volume in the bearing chamber gradually increases. However, for scheme A, with the increase of bearing rotation speed, the oil volume in the bearing first decreases and then increases under the oil velocity of 48m/s, which may be caused by unstable air pressure at high flow velocity. For scheme B, the internal oil volume changes evenly with bearing rotation speed. When oil velocity is 18m/s, the oil-phase volume in bearing cavity is the largest. Fig.7 (c) and Fig.7 (d) show the effect of oil velocity on oil-phase volume. The oil velocity is negatively correlated with the oil volume in bearing cavity, which means that the oil volume decreases as the oil velocity increases. When the bearing rotation speed is 10000r/min, the oil-phase volume in bearing cavity is the largest. Fig.7 (e) shows the oil storing rate in roller-sliding bearing chamber of scheme A.

Here, the oil storing rate η in bearing cavity is calculated as $\eta = [b/(a+b)] \times 100\%$, where a is the oil-phase volume in outer flow field and b is the oil-phase volume in bearing cavity. When the bearing

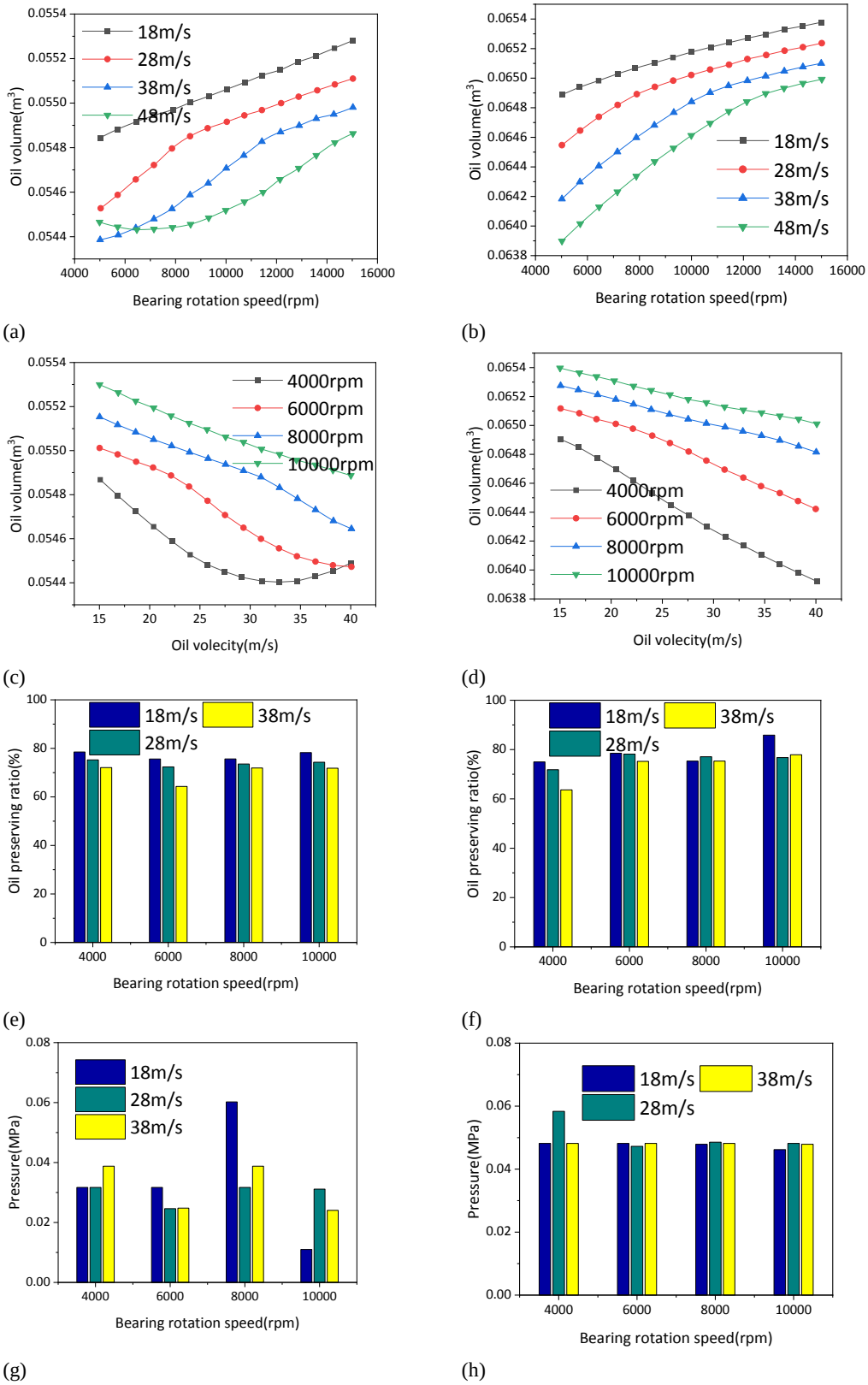

Fig. 7. Lubrication characteristics of the roller-sliding bearing at different oil velocities and bearing rotation speeds. (a) Effect of bearing rotation speed on the volume of oil-phase of scheme A; (b) Effect of bearing rotation speed on the volume of oil-phase of scheme B; (c) Influence of oil velocity on the volume of oil-phase of scheme A; (d) Influence of oil velocity on the volume of oil-phase of scheme B; (e) Oil storing rate in the roller-sliding bearing chamber of Scheme A; (f) Oil storing rate in the roller-sliding bearing chamber of Scheme B; (g) Average pressure on the slider of scheme A; (h) Average pressure on the slider of scheme B.

rotation speed is constant, the oil storing rate slightly decreases with the increase of oil velocity. When the oil velocity is 18m/s and the bearing rotation speed is 10000r/min, the oil storing rate is the highest. Fig.7 (g) shows the average pressure on slider of scheme A. The average pressure on slider surfaces is strongly influenced by bearing rotation speed. When the oil velocity is 18m/s and the bearing speed is 10000r/min, the pressure is lower than other three cases.

Figure 7 (f) illustrates the oil storing rate in roller-sliding bearing chamber of scheme B. The oil storing rate in bearing cavity varies with the bearing rotation speed. When the oil velocity is 18m/s and the bearing speed is 10000r/min, the rate of oil storing is the highest. Fig.7 (h) denotes the average pressure on the slider of scheme B. The average pressure on slider appears to be higher in scheme B compared to scheme A. However, there is a smooth pressure trend of slider in scheme B. In other words, scheme B has a stable pressure and the interaction between slider and roller is weakened. The slider can share some pressure for roller to a greater extent.

From the results in Fig. 7, it can be seen that the bearing speed and the oil speed have opposite effects on the oil-phase volume in the roller plain bearing, which is positively related to the bearing speed and negatively related to the oil velocity. Under the same working conditions, the oil-phase volume in the bearing cavity of scheme B has a more stable pressure trend on the slider surface, which is higher than that of scheme A. In scheme B, when the oil velocity is 18m/s and the bearing rotation speed is 10000r/min, there is a relatively higher oil storage rate and a lower pressure on the slider surface in relation to other working conditions. Therefore, the roller-sliding bearing has good lubrication characteristics in this case.

4.3 Influence of Oil Ratio and Oil Temperature on Bearing Lubrication Characteristics

Figure 8 describes the lubrication characteristics of roller-sliding bearing with different oil ratios and different oil temperatures. Here, the oil ratio is defined as $\lambda = c/(c+d)$, where c is the volume of oil-phase of inlet and d is the air-phase volume of inlet. In this section, the oil velocity is 18m/s. The oil viscosity and bearing rotation speed are 0.14Pa·s and 10000r/min, respectively. The oil ratio cases are 0.1, 0.3, 0.6, and 0.9, respectively. Meanwhile, the oil temperature cases are 20℃, 24℃, 28℃, 32℃, respectively. The oil ratio, oil temperature, oil storing rate in the bearing cavity, and pressure on the slider are considered. Fig. 8(a) and Fig. 8(b) illustrate the influence of the oil temperature on the volume of oil-phase of the bearing cavity. It is observed that the oil temperature has little effect on the volume of oil-phase in scheme A and scheme B. Fig. 8(c) and Fig. 8(d) show the effect of oil ratio on oil-phase volume. In comparison with scheme B, the volume of oil-phase in the bearing cavity of scheme A is more sensitive to the change of oil ratio. Fig. 8(e) gives the oil storing rate in roller-sliding bearing cavity of scheme A. The oil storage rate reaches a higher level when the oil temperature and oil ratio are 20°C and 0.9, respectively. Fig. 8(f) illustrates the oil storing rate in roller-sliding bearing cavity of scheme B. Compared with scheme A, the oil storing rate of scheme B is relatively higher in terms of maximum oil storing rate. The oil storage rate reaches the highest level when the oil temperature and oil ratio are 20°C and 0.9, respectively. Fig. 8(g) describes the average pressure on slider surface of scheme A. The maximum oil storage rate is considered in this case, where the oil temperature is 20℃ and the oil ratio is 0.9. For scheme A, the pressure on slider surface is the largest, but the oil storing rate reaches a higher level (according to Fig. 8 (e)), which may be due to the high air pressure inside the bearing at this time. Fig. 8(h) gives the average pressure on slider surface of scheme B. Compared with scheme A, when oil ratio is 0.9 and oil temperature is 20℃, the pressure on slider surface is relatively small in scheme B.

From the results in Fig. 8, it can be concluded that the oil temperature has little effect on oil-phase volume fraction in the bearing cavity. But the oil ratio has a greater influence on the change of oil volume. When oil temperature is 20℃ and oil ratio is 0.9, in comparison with scheme A, scheme B has the lower pressure on slider surface and the higher oil storing rate, which means the lubrication performance of roller-sliding bearing is better than other working conditions.

4.4 Influence of Oil Viscosity on Bearing Lubrication Characteristics

Figure 9 shows the bearing lubrication characteristics for different oil viscosities. The oil temperature is 20℃. The oil ratio and the bearing speed are 0.9 and 10000r/min, respectively. In addition, the oil viscosity cases are 0.02, 0.06, 0.10, and 0.14Pa·s, respectively. In this section, the oil viscosity, oil storing rate in the bearing cavity, oil-phase volume, and air pressure are considered. Fig. 9(a) and Fig. 9(b) show the effect of different viscosity cases on oil-phase volume. It can be observed that the viscosity of the oil has an certain effect on the volume of the oil phase within the bearing. However, the change of oil-phase volume in bearing cavity becomes more stable with the increases of oil viscosity. When the volume of oil-phase in bearing cavity is the largest, the oil viscosity case is 0.14Pa·s. According to the results of Fig. 9(a) and Fig. 9(b), the oil viscosity has a similar effect on oil-phase volume under the same working conditions. But the rate of change in oil volume is different. Compared with scheme A, the volume of oil-phase in the bearing cavity of scheme B is a larger one. Fig. 9(c) illustrates the oil storing rate for different oil viscosity cases. In terms of the influence of oil viscosity on oil storing rate of bearing cavity, scheme A and scheme B have similar changing trends. With the increases of oil viscosity, the oil storing rate in the bearing cavity slightly increases. The oil storing rate in bearing cavity is higher than in other cases when the oil viscosity case is 0.14Pa·s. Moreover, the scheme B has a higher rate of oil storing than scheme A. In other words, the lubricant volume in the bearing cavity of scheme B is

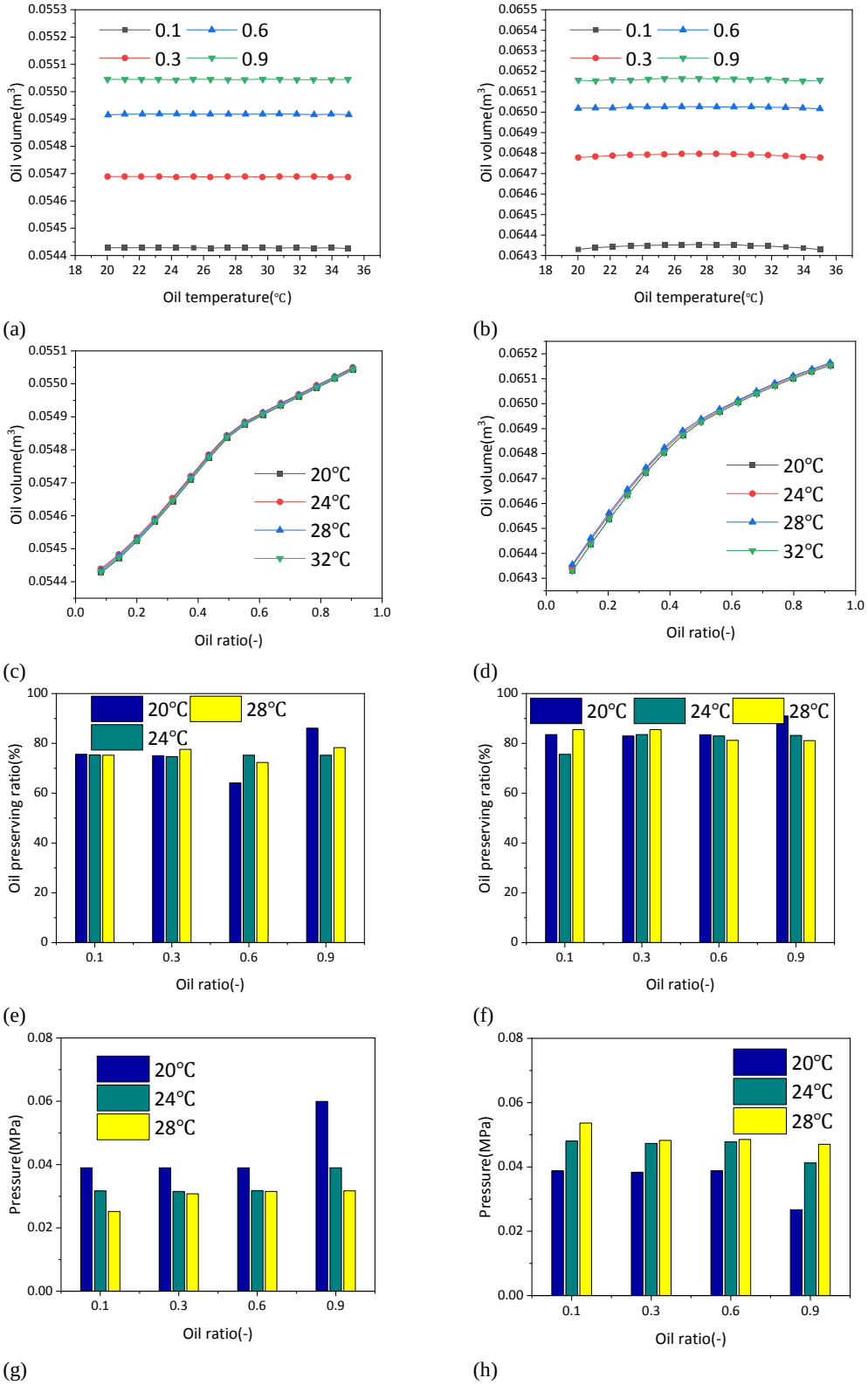

Fig. 8. Lubrication characteristics of roller-sliding bearing with different oil ratios and different oil temperatures. (a) Influence of oil temperature on oil-phase volume of scheme A; (b) Influence of oil temperature on oil-phase volume of scheme B; (c) Effect of oil ratio on oil-phase volume of scheme A; (d) Effect of oil ratio on oil-phase volume of scheme B; (e) Oil storing rate in roller-sliding bearing cavity of scheme A; (f) Oil storing rate in roller-sliding bearing cavity of scheme B; (g) Average pressure on slider surface of scheme A; (h) Average pressure on slider surface of scheme B.

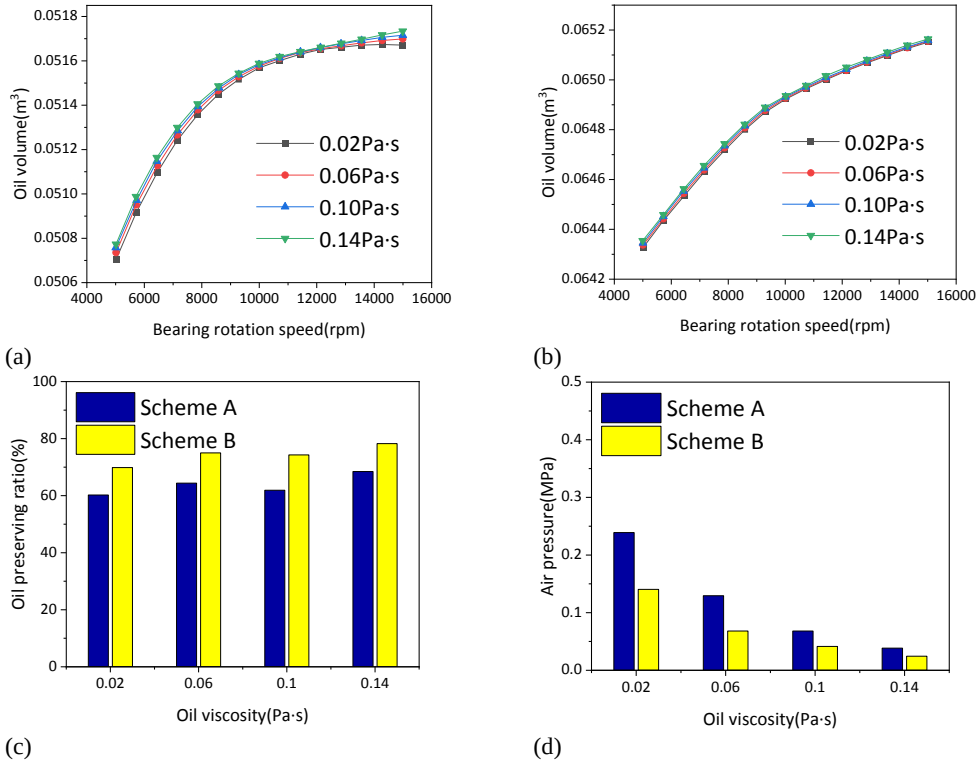

Fig. 9. Lubrication characteristics under different oil viscosity cases. (a) Effect of different viscosity cases on the volume of oil-phase of scheme A; (b) Effect of different viscosity cases on the volume of oil-phase of scheme B; (c) Oil storing rate for different oil viscosity cases; (d) Air pressure for different oil viscosity cases.

relatively larger. Therefore, it has better lubricating properties. Fig. 9(d) gives the air pressure for different oil viscosity cases. It can be found that the air pressure has the same trend of the changing with oil viscosity in the bearing cavity and the air pressure of scheme B is less than scheme A.

The viscosity of the oil has a relatively large impact on the air pressure in the bearing cavity according to the above analysis, which affects the lubrication performance of the bearing. For both design schemes, the oil viscosity has same influence trend on oil-phase volume in the bearing cavity. Moreover, the oil storing rate and air pressure in the bearing cavity will also be affected to a certain extent. When the oil viscosity case is 0.14Pa·s, compared with scheme A, scheme B has a larger oil volume, a higher oil storing rate and a lower air pressure, which means the lubrication performance is better in scheme B.

5. CONCLUSIONS

To investigate the lubrication characteristics of roller-sliding bearing under oil injection lubrication, the VOF model and CFD method are used to study the effects of bearing speed, oil velocity, oil temperature, oil viscosity, oil storing rate, slider pressure, and air pressure inside the bearing on the lubrication characteristics of the roller-sliding bearing. The following conclusions were drawn:

1. Under the condition of oil injection lubrication, the oil and gas distribution inside the rolling bearing was uneven. The volume fraction of the oil phase inside the bearing gradually increased from the inner raceway to the outer raceway and was lowest near the upstream of the nozzle due to the centrifugal force generated by the high-speed rotation of the bearing.

2. The influence of bearing speed and oil speed on the volume of the oil phase in roller-sliding bearing was the opposite. With the increase of the bearing speed, the oil phase volume inside the bearing gradually increased. However, as the oil supply speed increased, the oil phase volume inside the bearing gradually decreased.

3. Oil injection lubrication of roller-sliding bearing should consider the oil viscosity. The oil storing rate of the bearing cavity increased with the increase of the oil viscosity. As oil viscosity increased, the air pressure in the bearing cavity decreased.

4. The oil temperature had little impact on the oil-phase volume in the bearing cavity. When the bearing rotation speed case was 10000r/min, the oil velocity case was 18m/s, the oil temperature case was 20℃, the oil ratio case was 0.9, and the oil viscosity case was 0.14Pa·s. Compared with scheme A, scheme B had a higher oil storing rate in the bearing cavity, a higher oil storing rate, and lower pressure on the slider surface. Therefore, the lubrication performance of scheme B was better than other working conditions.

Furthermore, on the one hand, our future work will focus on the dynamic lubrication properties, computational rheology, and fluid heat transfer properties of high-speed roller-sliding bearings under oil injection lubrication conditions. On the other hand, there is a small gap between the slider and the raceway, so the near-wall meshing of the turbulent region will be the biggest challenge in the future. Therefore, in future studies, the author will further optimize the model to obtain more accurate results. Besides, as the oil ratio has a great influence on the complexity of fluid motion inside the roller-sliding bearing, the author will also consider the rheological behavior of the fluid in the roller-sliding bearing cavity to reveal the impact of non-Newtonian fluids on the lubrication characteristics of the roller-sliding bearing.

ACKNOWLEDGEMENTS

The authors want to thank anonymous reviewers for their helpful comments and suggestions to improve the manuscript and the help in the discussion from L. M. Lu in East China Jiaotong University. This research is supported by the research fund Science and Technology Key Project of Education Department of Jiangxi Province (GJJ190293) and National Natural Science Foundation of China (51065009).

REFERENCES

Awasthi, M. K., D. Yadav and G. S. Agrawal (2014). Viscous potential flow analysis of electrohydrodynamic Rayleigh Taylor instability. *Journal of Applied Fluid Mechanics* 7(2), 209-216.

Banerjee, R., K. M. Isaac, L. Oliver and W. Breig (2002). Features of automotive gas tank filler pipe two-phase flow: experiments and computational fluid dynamics simulations. *Journal of Engineering for Gas Turbines & Power* 124(2), 412-420.

Chao-Ho, H. and L. Rong-Tsong (1994). Advanced multilevel solution for elastohydrodynamic lubrication circular contact problem. *Wear* 177(2), 117–127.

Chu, L. M., H. C. Hsu, J. R. Lin and Y. P. Chang (2012). Inverse approach for the pressure, temperature, and pressure-viscosity index determination in TEHL of line contacts. *Industrial Lubrication and Tribology* 64(5), 294-302.

Chu, L., W. Li, Y. Chang and H. Hsu (2010). EHL of circular contacts lubricating with mixture of two lubricants. *Industrial Lubrication and Tribology* 62(2), 83-90.

Concli, F., C. T. Schaefer and C. Bohnert (2020). Innovative meshing strategies for bearing lubrication simulations. *Lubricants* 8, 1-14.

Da Riva, E. and D. Del Col (2012). Numerical simulation of laminar liquid film condensation in a horizontal circular minichannel. *Journal of Heat Transfer* 134(5), 51019-51019.

Feidt, M. (2012). Thermodynamics of energy systems and processes: a review and perspectives. *Journal of Applied Fluid Mechanics* 5(2), 85-98.

Gao, W., D. Nelias, K. Li, Z. Liu and Y. Lyu (2019). A multiphase computational study of oil distribution inside roller bearings with under-race lubrication. *Tribology International* 140, 1-10.

Harris, T. A. and M. N. Kotzalas (2006). *Rolling Bearing Analysis, fifth ed*., Taylor and Francis, New York.

Hirt, C. and B. Nichols (1981). Volume of fluid (VOF) method for the dynamics of free boundaries. *Journal of Computational Physics* 39 (1), 201-225.

Hu, J. B., W. Wu, M. X. Wu and S. H. Yuan (2014). Numerical investigation of the air-oil two-phase flow inside an oil-jet lubricated ball bearing. *International Journal of Heat and Mass Transfer* 68, 85-93.

Chu, L. M. (2010). Thin film elastohydrodynamic lubrication of circular contacts at pure squeeze motion. *Industrial Lubrication and Tribology* 62(4), 238-244..

Lu, L. M. (2013). Vibration characteristics of rolling-sliding blend bearing under the impact of cyclic loading, *Journal of Mechanical Engineering (China)*, 05, 39-46.

Lu, L. M., K. Gu, J. T. Tang, Z. H. Li and F. Li (2019). Finite element analysis of high speed and heavy-duty roller-sliding bearings. *Modular Machine Tool & Automatic Manufacturing Technique (China)* 07, 26-29+33.

Lu, L. M., Z. H. Li, F. Li and K. Gu (2020). Analysis of oil-gas two-phase flow lubrication on the slider of rolling-sliding bearing. *Lubrication Engineering* 45(5), 43-48.

Lu, L. M., Z. Niu, J. F. Lu and F. Li (2021). Simulation analysis of friction moment characteristic of rolling-sliding bearing, *Journal of Mechanical Transmission (China)* 45(09), 139-144.

Marchesse, Y., C. Changenet and F. Ville (2019). Drag power loss investigation in cylindrical roller bearings using CFD approach. *Tribology Transaction* 62, 403-11.

Mehdizadeh, A., S. A. Sherif and W. E. Lear (2011). Numerical simulation of thermofluid characteristics of two-phase slug flow in microchannels. *International Journal of Heat and Mass Transfer* 54(15-16), 3457-3465.

Meng, F. and Y. Chen (2015). Analysis of elasto-hydrodynamic lubrication of journal bearing based on different numerical methods.

Industrial Lubrication and Tribology 67(5), 486-497.

Ramdin, M and R. Henkes (2012). Computational fluid dynamics modeling of Benjamin and Taylor bubbles in two-phase flow in pipes. *Journal of Fluids Enginnering* 134(4), 1-8.

Wang, K., J. Wu and G. Zhao (2017). Numerical analysis of sliding bearing dynamic characteristics based on CFD. *Journal of Physics: Conference Series* 916, 012025.

Wei, L. D., H. J. Duan and Y. Zhang (2015). An EHD-mixed lubrication analysis of main bearings for diesel engine based on coupling between flexible whole engine block and crankshaft. *Industrial Lubrication and Tribology* 67(2), 150-158.

Wu, W., C. H. Hu, J. B. Hu and S. H. Yuan (2016), Jet cooling for rolling bearings: flow visualization and temperature distribution, *Applied Thermal Engineering* 105, 217–224.

Xiao, J. L., E. Q. Zhu and G. D. Wang (2012). Numerical simulation of emergency shutdown process of ring gate in hydraulic turbine runaway. *Journal of Fluids Engineering* 134(12), 1-9.

Zhang, Y. (2006). Contact-fluid interfacial shear strength and its critical importance in elastohydrodynamic lubrication. *Industrial Lubrication and Tribology* 58(1), 4-14.